Princeton Plasma Physics Laboratory

PPPL- 4870

PPPL- 4870

Geometrical Optics of Dense Aerosols

Michael J. Hay, Ernest J. Valeo and Nathaniel J. Fisch

April, 2013

PPPL PRINCETON PLASMA PHYSICS LABORATORY

Prepared for the U.S. Department of Energy under Contract DE-AC02-09CH11466.

Princeton Plasma Physics Laboratory
Report Disclaimers

Full Legal Disclaimer

Trademark Disclaimer

PPPL Report Availability

Princeton Plasma Physics Laboratory:

http://www.pppl.gov/techreports.cfm

Office of Scientific and Technical Information (OSTI):

http://www.osti.gov/bridge

Related Links:

U.S. Department of Energy

Office of Scientific and Technical Information

Fusion Links

Geometrical Optics of Dense Aerosols

Michael J. Hay,[1] Ernest J. Valeo,[2] and Nathaniel J. Fisch[1,2]

[1]*Department of Astrophysical Sciences, Princeton University, Princeton, New Jersey 08540*
[2]*Princeton Plasma Physics Laboratory, Princeton, New Jersey 08543*

(Dated: April 19, 2013)

Assembling a free-standing, sharp-edged slab of homogeneous material that is much denser than gas, but much more rarefied than a solid, is an outstanding technological challenge. The solution may lie in focusing a dense aerosol to assume this geometry. However, whereas the geometrical optics of dilute aerosols is a well-developed field, the dense aerosol limit is mostly unexplored. Yet controlling the geometrical optics of dense aerosols is necessary in preparing such a material slab. Focusing dense aerosols is shown here to be possible, but the finite particle density reduces the effective Stokes number of the flow, a critical result for controlled focusing.

Introduction.—Certain applications in plasma physics require a dense plasma slab, but preparing an appropriately dense, shaped, and homogeneous plasma *in vacuo* is difficult. Rapidly ionizing a very dense aerosol jet offers a promising path to such a plasma, but the physics of dense aerosols is entirely unexplored. In contrast, focusing effects in dilute aerosols have been the subject of extensive and fascinating work [1, 2]. The essential feature of the aerodynamic focusing of dilute aerosols is the formation of particle caustics as the flow passes through simple plate orifices, in analogy with geometrical optics. In the dense aerosol regime, this picture is modified by aberrations arising from the coupling of the particulate and continuous phases. This Letter accordingly departs from dilute calculations that treat the flow field and particle trajectories inconsistently by neglecting the finite particle momentum flux in the Navier-Stokes equations. In the process, we uncover new phenomena unique to the dense aerosol regime.

Dense Aerosol Regime.—To describe these phenomena, we envision a two-stage device (Fig. 1) that assembles a dense jet of particulate from a dilute, isotropic suspension. For concreteness, we specialize to a rectangular lens geometry with slit lenses and aerosol sheets. Passing through the first stage, the aerosol is focused into a narrow jet. Although the nozzle is subsonic and the carrier flow is essentially incompressible, the aerosol particles themselves are highly supersonic with respect to their Brownian motion: immense compression is possible [1]. In order to prepare sufficiently high-density plasma targets, the aerosol phase will necessarily carry mass comparable to the carrier fluid even prior to focusing.

In the dilute limit, focusing requires Stokes number $\mathrm{S} \doteq \tau u_o/L_o \simeq 1$, where u_o and L_o are the speed and transverse width of the flow at the subsonic orifice, and $\tau \doteq (2\rho_0 a^2/9\mu)(C_s/f_d)$ is the momentum relaxation time [2, 3]. ρ_0 is the bulk density of the particle material, a the radius of the spherical particles, μ the fluid viscosity, and $C_s \doteq 1 + (\lambda/a)[A_1 + A_2\exp(-A_3 a/\lambda)]$ is the Cunningham correction for particle slip ($\lambda \propto 1/\rho_g$ is the gas-gas mean free path and the A_i's are order unity constants). $f_d \sim \mathcal{O}(1)$ corrects for finite particle Reynolds number. Additionally, unless the Reynolds number $\mathrm{Re} \doteq \rho_g u_o L_o/\mu \lesssim 10^3$, the resulting turbulent flow is expected to disrupt the deterministic particle trajectories and inhibit focusing. The difference in cross-section between the first and second stage orifices $L_o/L_n \leq L_o/L_a$ is limited by the contraction of the aerosol beam to a factor $\lesssim 10$. Then the flow entering the second stage must exceed a certain Mach number $\gtrsim 0.01$ to reach the sonic point there. Operating at large Knudsen number $\mathrm{Kn} \doteq \lambda/a$ subsumes the Reynolds and Mach constraints. In that regime,

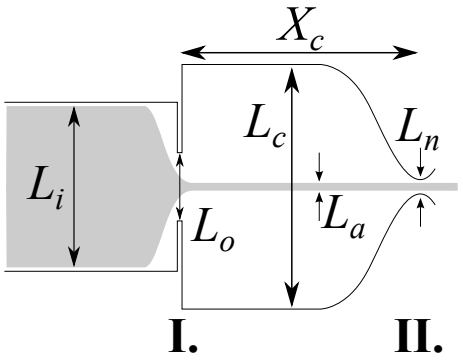

FIG. 1. Schematic of two-stage system for compressing and extracting aerosol targets (gray). Stage I forms a jet from the isotropic suspension at the inlet. Stage II extracts this jet by dispersing the carrier fluid.

$$\mathrm{S} \simeq 0.70\sqrt{\gamma}\frac{a\rho_0}{L_o\rho_g}\mathrm{M}_o \tag{1}$$

$\mathrm{M}_o = u_o/c_g$ is the subsonic orifice Mach number and we have taken $\mu = \bar{u}\lambda\rho_g/3$.

Together, these constraints on S, Re, and Kn impose an upper limit on the carrier fluid density. The desired plasma electron density n_e determines the mean mass density of the spheres, $\bar{\rho}_a = n_e(A/Z)M_p$, and therefore

$$\frac{\bar{\rho}_a}{\rho_g} \gtrsim 51\frac{L_o}{1\text{ cm}}\sqrt{\frac{1\ \mu\text{m}}{a}\cdot\frac{1\ \text{g/cm}^3}{\rho_0}}\left(\frac{n_e}{10^{19}/\text{cm}^3}\right) \tag{2}$$

In a homogeneous target ($n_a^{-1/3}/L_a < 10^{-2}$) suitable for

compression of micron light, each factor will be order unity.

Aerodynamic Focusing.—Several features of aerodynamic focusing were clarified by finite-volume ANSYS FLUENT calculations. In the dilute regime, focusing was found to depend on not only the particle S, but also the flow Re. Passing through a simple slit orifice, the contraction of the aerosol beam L_a/L_o exhibited a $\mathrm{Re}^{-1/4}$ dependence. This result was used to consistently determine operating points over several decades in Re.

Operating at finite ρ_a/ρ_g introduces aberrations that together result in lower-S focusing behavior as compared with a dilute flow of identical particles. As the tableau of simulations in Fig. 2 indicates, focusing shifts to larger particles; the effect is small for upstream $\rho_a/\rho_g \sim \mathcal{O}(1)$. Fig. 2a shows S ≈ 0.9 particles focusing tightly in the upper half of the channel. The velocity field and particle tracks have been calculated by FLUENT in the dilute limit, $\rho_a/\rho_g \doteq \rho_p/\rho \approx 0.001$. Asymptotically, there is very little widening of the envelope of particle trajectories. Fig. 2b traces identical particles with significant momentum coupling between the continuous and discrete phases, resulting in a divergent stream. Under mass loading, the orifice flow velocity is lowered by acceleration of the aerosol phase, reducing Re. Likewise, the contraction of the aerosol flow can compress the carrier gas, thereby altering the streamline curvature. The energetic aerosol particles subsequently increase the axial carrier velocity above the dilute calculation downstream of the orifice, resulting in the small-divergence trajectories traced in Fig. 2b. Comparing Fig. 2c, it is evident that increasing S at high mass loadings can reduce the sheet's divergence downstream of the orifice. In both cases, the relatively dilute edge of the beam has the greatest divergence angle due to drag on the carrier flow filling the channel. Fig. 2d traces the larger particles' paths in the dilute limit, confirming that adjusting S is responsible for the change in dynamics. At finite S, the beam nevertheless tends to a negligible divergence far downstream due to the underlying Poiseuille flow. The slight defocusing effect of finite mass loading is not included consistently within the calculation of two-stage operating points; the particle trajectories between stages were assumed to have zero divergence before entering the second stage.

Coagulation.—The most severe operating constraint on the two-stage device is particle coagulation, which occurs upon a collision or approach within a distance characteristic of the van der Waals force. Upstream of the first stage, coagulation can destroy focusing and contribute to particle loss by altering the distribution of particle sizes. Downstream, where the residence time is very long and the particle density is high on-axis, coagulation reduces the homogeneity of the jet. The constraint pushes the operating regime to larger a, smaller L_a, and lower ρ_a.

The need for good homogeneity at high focused densities motivates operation in a regime where the effective scattering length l_B of an aerosol particle's Brownian motion is large compared to a: $l_B \doteq v_{th}\tau \gtrsim a$, where $v_{th} \simeq \sqrt{T_g/m_p}$. This results in a longer collision time due to Knudsen flow in a layer of radial extent l_B surrounding each aerosol particle [4]. The particle residence time cf. the local collision rate is longest between stages, so the constraint is determined there:

$$\frac{\tau_{\mathrm{transit}}}{\tau_{\mathrm{coag}}} \simeq \frac{X_c/u_c}{\tau_{\mathrm{coag}}} < 1 \tag{3}$$

where u_c is the gas speed in the central region and [4]

$$\tau_{\mathrm{coag}} \simeq (2\sqrt{2}\pi n_a a^2 v_{th}\delta)^{-1} \tag{4}$$

where $n_a \doteq \rho_a/m_p$ is the number density of spheres. $\delta \leq 1$ is the fraction of collisions resulting in coagulation: a measure of the aerosol material's van der Waals interaction strength. Note the strong dependence on particle size: $\tau_{\mathrm{coag}} \propto a^{5/2}$ at fixed ρ_a.

Target Density and Aspect Ratio.—We assume fluid descriptions for the coupled gas and aerosol flows in order to calculate the focused target's density and divergence. Although the particle Knudsen number is large, the criterion for continuum flow is easily satisfied: $\lambda/L_o \ll 1$. Because the particle volume fraction $\rho_a/\rho_0 \ll 1$, the body force coupling the two fluids is $\propto \rho_a(\mathbf{u}_a - \mathbf{u}_g)/\tau$. Within the focused aerosol beam, $\rho_a/\rho_g \gg 1$ and we may neglect the inertial part of the gas momentum equation to obtain:

$$\mathbf{u}_g \simeq \mathbf{u}_a - \frac{\tau}{\rho_a}\nabla p_g \tag{5}$$

Assuming an equation of state $p_g = p_g(\rho_g)$, the gas continuity equation has the convection-diffusion form:

$$\frac{\partial \rho_g}{\partial t} + \nabla\cdot\rho_g\mathbf{u}_a = \nabla\cdot\frac{\tau}{\rho_a}\rho_g c_g^2\nabla\rho_g \tag{6}$$

where $c_g^2 = \partial p_g/\partial\rho_g$. Near the subsonic orifice, the aerosol compression of order L_i/L_o can drive a corresponding $\Delta\rho_g$. In steady state, the gas diffusion compensates the convective aerosol compression:

$$\rho_g\frac{\hat{\mathbf{y}}\cdot\mathbf{u}_a}{L_o} \sim \frac{\tau\rho_g c_g^2}{\rho_a L_o^2}\Delta\rho_g \tag{7}$$

where $\hat{\mathbf{y}}$ is the transverse flow direction. Then

$$\frac{\Delta\rho_g}{\rho_g} \sim \alpha \doteq \frac{2L_o^2}{\gamma a^2}\cdot\frac{\rho_a\rho_g}{\rho_0^2} \ll 1 \tag{8}$$

if we can neglect the carrier gas compressibility. This is a consistency condition for the two-fluid model: $\alpha < 1$ restricts particle trajectory crossings due to coherent hydrodynamic motion. Crossings due to random motion

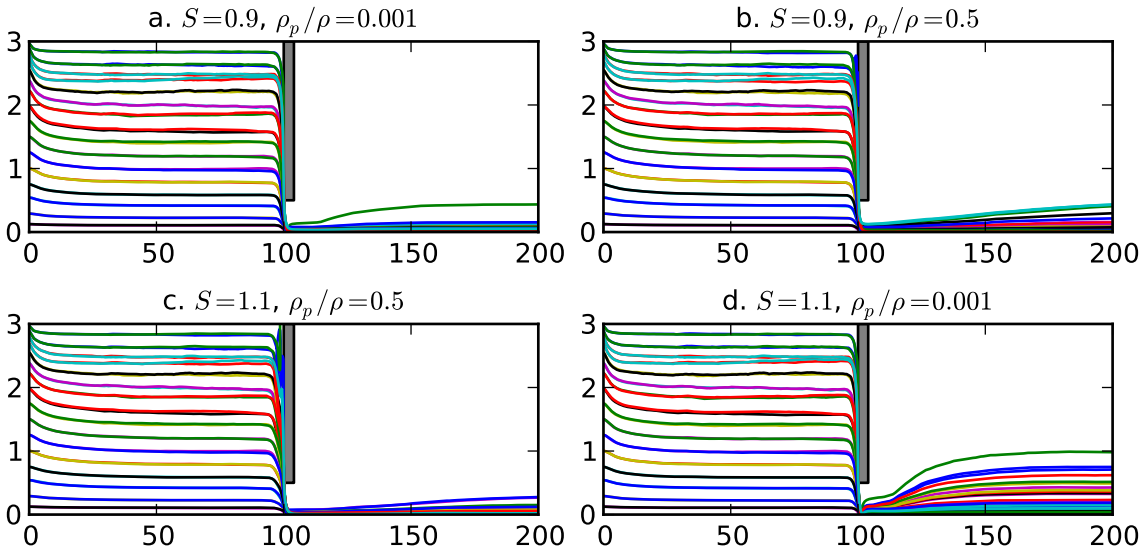

FIG. 2. Representative particle tracks demonstrating aerodynamic focusing in four combinations of S and injection ρ_p/ρ. In each frame, the abscissa is the horizontal displacement in multiples of w_o; the ordinate is the vertical displacement. The axial extent of the orifice is exaggerated for clarity.

(i.e. coagulation) are explicitly constrained per inequality (3). If $\alpha \ll 1$, the radial diffusion of gas in the focused beam is faster than axial convection viz.

$$\nu_\perp \sim \frac{\tau \rho_g c_g^2}{\rho_a L_a^2} \gg \hat{\mathbf{x}} \cdot \mathbf{u}_a \frac{d}{dx} \log L_a \sim \nu_\parallel \tag{9}$$

and $\partial \rho_g / \partial y$ is accordingly negligible. Then $L_a \simeq$ const. and the summed momentum equations for the two phases have a first integral:

$$\frac{S_a}{L_a} u_a + p_g(\rho_g) \doteq \text{const.} \tag{10}$$

where $S_a \doteq \rho_a u_{a,x} L_a \simeq$ const. In the limit of large downstream Mach number, $p_g \to 0$ and Eq. (10) implies that

$$u_{a,f} \leq \frac{L_a}{S_a} p_{g,i} \tag{11}$$

where $u_{a,f}$ is the final downstream aerosol speed and $p_{g,i}$ is the gas pressure far upstream of the focusing device. The acceleration of the aerosol beam is limited by a 'barreling' effect that depends on the contrast ratio ρ_a/ρ_g.

As $\rho_g(x)$ decreases through the supersonic nozzle, a transverse pressure gradient $\partial p_g/\partial y$ is established that can in turn develop a diverging $u_{a,y}$. Comparing the axial convection and radial diffusion terms of Eq. (6),

$$u_{a,x} \frac{\partial \rho_g}{\partial x} \sim \frac{\partial}{\partial y} \frac{\tau \rho_g c_g^2}{\rho_a} \frac{\partial \rho_g}{\partial y} \tag{12}$$

and substituting the y-component of the summed momentum equations,

$$\rho_a u_{a,x} \frac{\partial u_{a,y}}{\partial x} = -c_g^2 \frac{\partial \rho_g}{\partial y} \tag{13}$$

we estimate the divergence as

$$\frac{u_{a,y}}{u_{a,x}} \sim \frac{L_a/\tau}{u_{a,x}} \simeq \frac{L_a}{L_o} \alpha^{1/2} \tag{14}$$

where we have estimated $\partial/\partial y \sim 1/L_a$ and $u_{a,x} \sim (\rho_g/\rho_a)^{1/2} v_{th}$ from Eq. (11). The upper bound on the aerosol speed also provides an estimate of the extracted target density:

$$\frac{\rho_t}{\rho_{a,i}} \simeq \frac{L_i u_i}{L_a u_{a,f}} = \frac{L_o^4 (\rho_a \rho_g)_i}{a^2 L_a^2 \rho_0^2} = \frac{L_o^2}{L_a^2} \alpha \tag{15}$$

where we have used S = 1 to eliminate the upstream gas velocity u_i.

$\alpha \ll 1$ is a consistency criterion for the two-fluid model, but the final target density is small in this limit. Alternately, the target aspect ratio scales as $\alpha^{-1/2}$; intermediate α is necessary for high-quality targets. It is more important to operate in a large L_o/L_a regime, which occurs for S = 1 and Re $\gtrsim 10^2$. In order to safely compress high-fluence beams and subsequently attain large geometric convergence, large aspect ratio geometries are necessary. We estimate $AR \geq 10$ to be satisfactory, well in excess of what is available with gas jets. These and the aforementioned constraints are catalogued in Table 1.

Operating Points.—The operating space accessible with a two-stage device is restricted by the enumerated constraints. Considering $n_e \simeq 10^{19}$ cm^{-3} plasmas suitable for Raman compression, the available targets are charted in Fig. 3. In particular, we note that 5-mm targets are available with good homogeneity: $a/L_a \sim 10^{-5}$. Due to the M = 1 constraint at the supersonic nozzle

Stage I	$\mathrm{S} \simeq 1$
	$\mathrm{Re} < 10^3$
	$\alpha \ll 1$
	$\mathrm{M}_o \doteq u_o/c_g < 0.3$
	$\mathrm{Kn} \doteq \lambda/a > 1;\ \lambda/L_o \ll 1$
Between stages	$X_c \gtrsim 5L_o$
	$L_c > L_a$
	$X_c/u_c < \tau_{\mathrm{coag}}$
	$l_B/a > 1$
Stage II	$\mathrm{M}_n = 1$
	$L_n > L_a$
	$AR \doteq (L_a\alpha^{1/2}/L_o)^{-1} > 10$
	$n_a^{-1/3}/L_a < 10^{-2}$
	$\rho_t \simeq 0.017(\frac{A}{Z})\left(\frac{n_e}{10^{19}/\mathrm{cm}^3}\right)\ \mathrm{mg/cm}^3$

TABLE I. Dense aerosol operating constraints

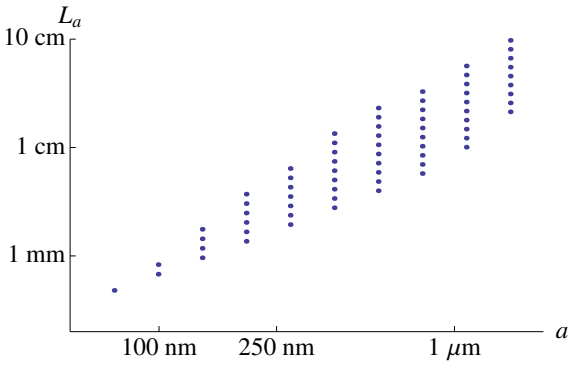

FIG. 3. Possible operating points at $n_e \simeq 10^{19}\ \mathrm{cm}^{-3}$ in $(a,\, L_a)$ space. Each point is parametric in Re and M.

throat, the largest allowed Reynolds number sets the maximum aerosol particle size. Independent of L_a and ρ_t, $a < 0.34\mathrm{Re}^{3/2}$ nm. The minimum a is set by the coagulation constraint:

$$a > 2\ \mathrm{nm}\left(\frac{1}{\mathrm{M}^3}\cdot\frac{L_a}{1\ \mathrm{mm}}\cdot\frac{n_e}{10^{19}\ \mathrm{cm}^{-3}}\right)^{1/4} \tag{16}$$

where M is the maximum Mach number allowed. At fixed a, small-L_a targets below the boundary identified in Fig. 3 are too inhomogeneous. Likewise L_a above the region in Fig. 3, require high-M and high-Re operation that could result in deleterious shocks, turbulence, etc. At fixed (a, L_a), a higher-density target is subject to those constraints; the (a, L_a) operating space tends to widen as ρ_t is reduced. Perhaps the most promising aspect of this device is the possibility of forming structured targets (e.g. by slight defocusing, $\mathrm{S} \approx 1$) which offers a straightforward path to detuned amplification via plasma density gradients [5].

Alternative Techniques and Applications.—Alternative techniques for producing a plasma slab suffer from limitations that might be overcome using the dense aerosol approach. Aerogels and foams are characterized by filamentary structures and pores on the nm scale. These filaments are responsible for the material structure and strength and so contribute an intrinsic anisotropy, limiting amplification. In laser plasmas, the timescales over which the filaments vaporize and the target material homogenizes must be much shorter than the hydrodynamic timescale for the target edge to rarefact and expand. Because a typical filament has a large aspect ratio, it expands in 2D and such structures can persist late in the ionizing pulse [6, 7]. Gas jets lack a solid matrix but are instead saddled with short hydrodynamic timescales associated with turbulent eddies and the propagation of shocks from the nozzle.

One important application of dense aerosol targets is fast Raman compression, which requires good uniformity at high electron densities [5]. Low-divergence aerosol targets could surpass the efficiencies of gas jets in radiator experiments on Z [8]. However, the homogeneity and aspect ratio requirements are relaxed somewhat compared to those required for Raman compression; here, a satisfactory design point is a 1-cm jet of 10-μm nickel particles, $\rho_0 = 8.9\ \mathrm{g/cm}^3$. Larger particles are less susceptible to coagulation; the Reynolds constraint (2) guarantees operation in a moderately dense aerosol regime: $\rho_a/\rho_g \gtrsim 10^2$ at $10^{19}\ \mathrm{cm}^{-3}$. Similar dense aerosol schemes could offer structured targets to the MagLIF program, which is expected to rely on laser heating of annular targets [9].

Summary.—Self-consistent momentum coupling between aerosol and carrier flows changes the aerodynamic focusing properties of the system. The addition of particle density to converging flows contributes a spherical aberration to the focus; in the first stage, finite particle density reduces the effective Stokes number of the flow. In the resulting dense jet, the aerosol determines the local flow field; in the second stage, the particles move ballistically despite their large slip velocities.

The deterministic focusing properties of aerodynamic lenses permit the design of homogeneous, high-aspect ratio targets that permit the compression of light at lower intensities and substantial geometric convergence. Jets of small spherical particles could be engineered to homogenize quickly with minimal turbulent features. Because so many solid and liquid species can be aerosolized, these targets open up the design space for plasma technologies. Separating the target's assembly and ionization permits complex designs with tailored gradients that could improve current plasma technologies.

This work was performed under DOE contract number DE-AC02-09CH11466. One of us (MJH) was supported by the DOE NNSA Stewardship Science Graduate Fellowship under grant number DE-FC52-08NA28752.

[1] J. F. de la Mora and P. Riesco-Chueca, J. Fluid Mech. **195**, 1 (1988).

[2] P. Liu, P. J. Ziemann, D. B. Kittelson, and P. H. McMurry, Aerosol Sci. Technol. **22**, 293 (1995).

[3] X. F. Zhang, K. A. Smith, D. R. Worsnop, J. Jimenez, J. T. Jayne, and C. E. Kolb, Aerosol Sci. Technol. **36**, 617 (2002).

[4] N. A. Fuchs, *The Mechanics of Aerosols* (MacMillan, New York, 1964).

[5] V. M. Malkin, G. Shvets, and N. J. Fisch, Phys. Rev. Lett. **84**, 1208 (2000).

[6] A. E. Bugrov, S. Y. Gus'kov, V. B. Rozanov, I. N. Burdonskiĭ, V. V. Gavrilov, A. Y. Gol'tsov, E. V. Zhuzhukalo, N. G. Koval'skiĭ, M. I. Pergament, and V. M. Petryakov, JETP **84**, 497 (1997).

[7] G. J. Caporaso, Phys. Fluids **25**, 436 (1982).

[8] H. Sze, J. Banister, B. H. Failor, J. S. Levine, N. Qi, A. L. Velikovich, J. Davis, D. Lojewski, and P. Sincerny, Phys. Rev. Lett. **95**, 105001 (2005).

[9] S. A. Slutz and R. A. Vesey, Phys. Rev. Lett. **108**, 025003 (2012).

The Princeton Plasma Physics Laboratory is operated
by Princeton University under contract
with the U.S. Department of Energy.

Information Services
Princeton Plasma Physics Laboratory
P.O. Box 451
Princeton, NJ 08543

Phone: 609-243-2245
Fax: 609-243-2751
e-mail: pppl_info@pppl.gov
Internet Address: http://www.pppl.gov